Lithos 206–207 (2014) 65–78

Contents lists available at ScienceDirect

Lithos

journal homepage: www.elsevier.com/locate/lithos

Petrogenesis of the early Cretaceous intermediate and felsic intrusions at the southern margin of the North China Craton: Implications for crust–mantle interaction

Xin-Yu Gao, Tai-Ping Zhao *, Zhi-Wei Bao, Alexandra Yang Yang

Key Laboratory of Mineralogy and Metallogeny, Guangzhou Institute of Geochemistry, Chinese Academy of Sciences, Guangzhou 510640, China

ARTICLE INFO

Article history:
Received 17 December 2013
Accepted 10 July 2014
Available online 30 July 2014

Keywords:
Early Cretaceous magmatism
Geochemistry
Petrogenesis
Southern margin of the North China Craton

ABSTRACT

New major and trace element, whole rock Sr and Nd isotopes and zircon U–Pb ages and Hf isotope data are presented for rocks from the early Cretaceous Tianqiaogou dioritic and Taishanmiao granitic plutons at the southern margin of the North China Craton (NCC), in order to investigate their petrogenesis and geological evolution. LA-ICP-MS U–Pb analyses for zircons from these two plutons yield similar $^{206}Pb/^{238}U$ ages of 122 Ma and 115–125 Ma, respectively. Monzodiorites from the Tianqiaogou pluton have whole rock $\varepsilon_{Nd}(t)$ values ranging from −6.2 to −1.3 and zircon $\varepsilon_{Hf}(t)$ values from +2.9 to +6.2. They are variably enriched in Ra, Ba, and Sr, and depleted in Nb, Ta, Zr, Hf and Ti, indicating that they were derived from a depleted mantle and underwent subsequent magma differentiation and crustal contamination. The Taishanmiao pluton is composed of metaluminous to peraluminous highly fractionated I-type granites that have high SiO_2, Na_2O, K_2O, Rb, Th, and U, and low P, Ba, Sr, Ti and Eu contents. The granites have strong negative whole rock $\varepsilon_{Nd}(t)$ values (−16.1 to −7.5) and zircon $\varepsilon_{Hf}(t)$ values (−20.9 to −6.1). Their Nd T_{DM} ages (1.19 to 2.01 Ga) and zircon Hf *T*C DM ages (1565 to 2490 Ma) are much younger than the basement rocks beneath the southern margin of the NCC, suggesting derivation from an ancient crustal source with minor involvement of mantle-derived components. Therefore, rocks from the Tianqiaogou dioritic pluton were partial melts of the mantle source. Underplating of the mafic magmas initiated partial melting of the ancient continental crust, resulting in the formation of the Taishanmiao granitic pluton. Their complex petrogenesis reflects a strong crust–mantle interaction process related to lithospheric thinning beneath the southern margin of the NCC in early Cretaceous.

© 2014 Elsevier B.V. All rights reserved.

1. Introduction

It has been generally considered that the North China Craton (NCC) underwent craton destruction and lithospheric thinning during the late Mesozoic (e.g. Gao et al., 2004; Wu et al., 2005; Zhang, 2012; Zhang et al., 2013; Zheng et al., 2007). More than 100 km of the ancient lithosphere may have been removed beneath the NCC, and this was accompanied by voluminous mafic to felsic magmatism and large-scale Mo–Au–Ag polymetallic mineralization (e.g. Chen et al., 1998; Goldfarb and Santosh, 2014; Guo et al., 2013; J.W. Li et al., 2012; Li and Santosh, 2014; Mao et al., 2011; Zhai and Santosh, 2013). The igneous rocks along the southern margin of the NCC are important for constraining their spatial and genetic relationships with ore deposits (e.g. Mao et al., 2011), crust–mantle interaction and the tectonic evolution of the NCC (e.g. Mao et al., 2010).

The late Mesozoic granites along the southern margin of the NCC are thought to have been derived from ancient continental crust of the NCC (e.g. Ding et al., 2011; Gao et al., 2010; N. Li et al., 2012; Zhao et al., 2012; Zhu et al., 2013) or from the subducted Yangtze Craton (e.g. Bao et al., 2014). There is a consensus that underplating of the mantle-derived magmas triggered partial melting of the lower crust (Bergantz, 1989; Y.G. Xu et al., 2009). Nevertheless, it remains unclear whether and to what extent mantle-derived components were involved in the petrogenesis of the granitic magmas in the southern margin of the NCC during the late Mesozoic (Ding et al., 2011; N. Li et al., 2012; Zhao et al., 2012) due to lack of evidence of contemporaneous mantle-derived magmatic activity. The key to these debates is to identify primary granites and associated intermediate to mafic rocks. The sparsely distributed mafic intrusions in the southern margin of the NCC may bear information of the geochemical composition of the mantle and regional tectonic evolution. However, the genetic relationships between the temporally and spatially coexisting granitic rocks and the intermediate to mafic rocks in this region are still unknown.

Late Mesozoic granitoid intrusions in the southern margin of the NCC were formed in two main magmatic intervals, the late Jurassic to early Cretaceous (ca. 160–135 Ma) and the early Cretaceous (ca. 130–110 Ma), in distinct tectonic settings (Mao et al., 2010). Many researchers have demonstrated that the 160–135 Ma adakitic granites were produced by partial melting of thickened lower continental crust

* Corresponding author. Tel.: +86 20 85290231; fax: +86 20 85290130.
E-mail address: tpzhao@gig.ac.cn (T.-P. Zhao).

http://dx.doi.org/10.1016/j.lithos.2014.07.019
0024-4937/© 2014 Elsevier B.V. All rights reserved.

(Ding et al., 2011; Gao et al., 2010; N. Li et al., 2012b; Zhao et al., 2012). However, the 130–110 Ma granites are geochemically different from the adakites, and have not yet been well-documented (Ye et al., 2008). The latter offers important information about the evolution of continental crust and specific tectonic regimes.

In this paper, we report geochronological and geochemical data for the Tianqiaogou dioritic and the Taishanmiao granitic plutons in the Waifangshan area of the southern margin of the NCC, to investigate their petrogenesis and tectonic implications, as well as to explore the possible crust–mantle interaction related to the Mesozoic lithospheric thinning beneath the NCC.

2. Geological background

The North China Craton is bordered by the Central Asian Orogenic Belt to the north, the Qinling–Dabie Orogenic Belt to the south and the Su–Lu Orogenic Belt to the east (Fig. 1A). The southern margin of the NCC is generally confined by the Sanmenxia–Lushan Fault to the north and Luonan–Luanchuan Fault to the south (Fig. 1B). The region shares the same basement-cover sequence to the NCC, namely the Archean to early Paleoproterozoic basements and the overlying late Paleoproterozoic to Phanerozoic unmetamorphosed cover sequence.

The basement of the southern margin of the NCC is represented by the Neoarchean–Paleoproterozoic Taihua Group (2.26–2.84 Ga) that is composed of metamorphic rocks, such as amphibolite, felsic gneiss, migmatite, and metamorphosed supracrustal rocks (Kröner et al., 1988; Wan et al., 2006; X.S. Xu et al., 2009). The Taihua Group is unconformably overlain by the Xiong'er Group that is up to 7600 m thick and covers an area of >60,000 km^2 (Zhao et al., 2004). The Xiong'er Group formed in the period of 1.75–1.78 Ga (Zhao et al., 2004) and consists mainly of intermediate to acidic lavas and pyroclastic rocks intercalated with minor sedimentary rocks (<5%). The Xiong'er Group is covered by the Meso- to Neoproterozoic sedimentary rocks of the Guandaokou and Luanchuan Groups. The southern margin of the NCC lacks Paleozoic–Jurassic strata and no Jurassic rocks can be observed (Fig. 1B). Since the beginning of the Cretaceous, lacustrine or alluvial sediments began to develop in the region.

Granitic rocks are widespread on the southern margin of the NCC. The Precambrian granitic rocks include the Neoarchean (2.9–2.5 Ga) tonalite–trondhjemite–granodiorite (TTG) gneiss, Paleoproterozoic

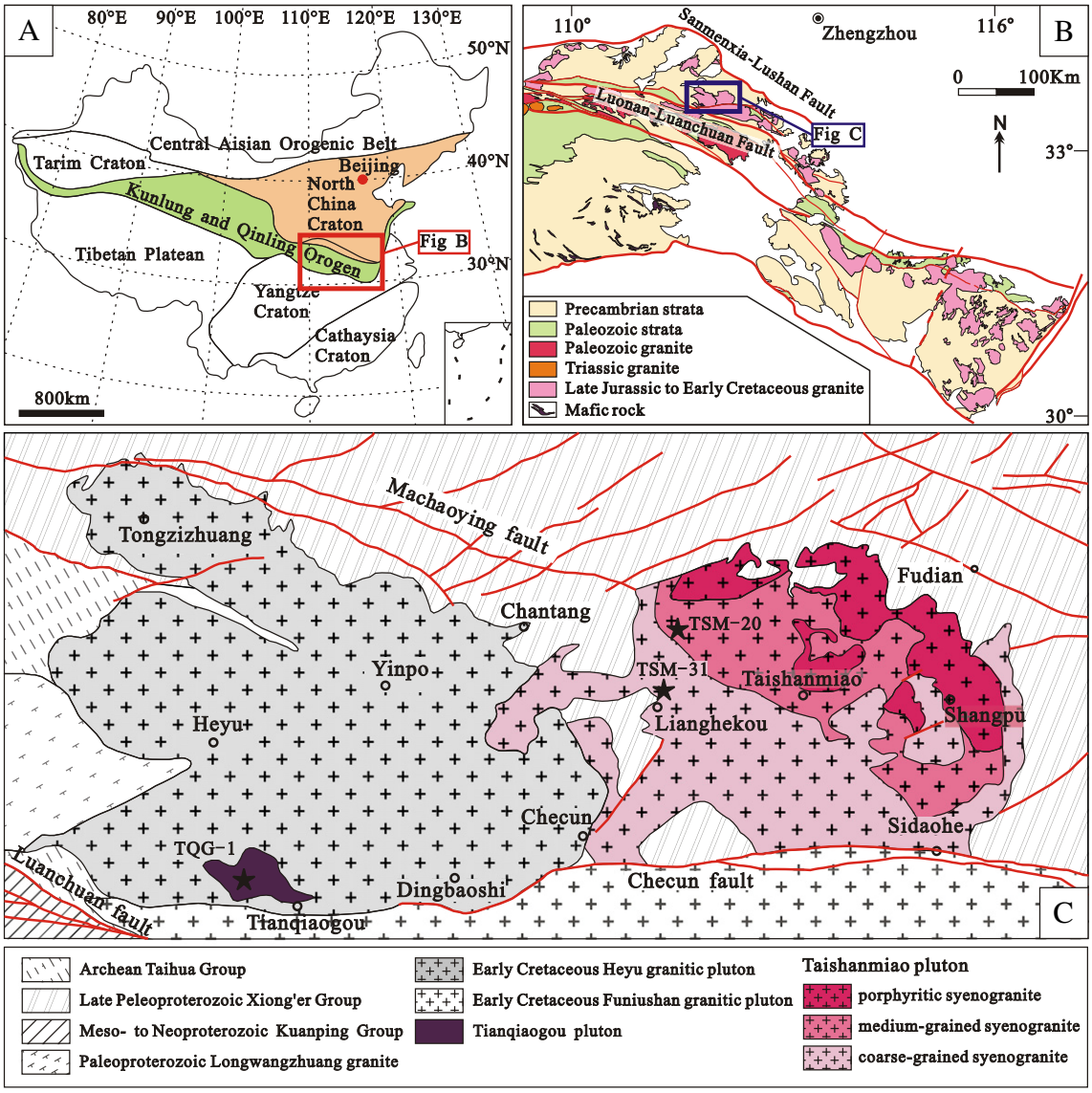

Fig. 1. Geological map in Waifangshan area, southern margin of the North China Craton. (A) Simplified tectonic map of China showing major tectonic phases surrounding the North China Craton and the location of the Qinling Orogen Belt. (B) Geological map of the Qinling Orogen Belt (modified from Zhang et al., 1996). (C) Geological map of the early Cretaceous intrusion in Waifangshan area.

(2.4–1.6 Ga) monzonitic and alkaline granite, late Mesoproterozoic to early Neoproterozoic (1.1–0.8 Ga) monzogranite and granitic pegmatite and the Late Mesozoic granitic plutons and Mo-mineralized granite porphyries (160–110 Ma). They intruded into the Archean amphibolite facies metamorphic rocks or Proterozoic to early Paleozoic unmetamorphosed volcanic–sedimentary sequences throughout the southern margin of the NCC (Fig. 1B) (Mao et al., 2010).

The mafic intrusions in this region, dominated by mafic dykes or stocks, were mainly emplaced the Archean metamorphic rocks during Mesoproterozoic (Peng et al., 2008), and sporadically during late Mesozoic (Wang et al., 2008). The late Mesozoic mafic rocks are mainly composed of dolerite and diorite with minor lamprophyre, with SHRIMP zircon U–Pb ages of ~128 Ma (Wang et al., 2008).

3. Field occurrence and petrography

The Taishanmiao pluton intruded into the intermediate to acidic volcanic rocks of the Jidanping Formation from the Paleoproterozoic Xiong'er Group to the northeast (1.75–1.78 Ga; Zhao et al., 2004) and into the early Cretaceous Heyu granitic pluton to the west (148–134 Ma; Gao et al., 2010; Li et al., 2012b), and separated by the early Cretaceous Funiushan pluton to the south by the Checun fault (Fig. 1C). The Taishanmiao pluton contains abundant xenoliths from the country-rocks, most of which were rhyolites and andesites from the Xiong'er Group. The xenoliths are rounded or irregular in shape, ranging from few centimeters to several meters in size, and have sharp boundaries.

The Taishanmiao pluton, covering an area of 290 km^2 (Fig. 1C), was produced by three episodes of magmas. The rocks are mainly composed of medium- to coarse-grained syenogranites and porphyritic syenogranites. The coarse-grained syenogranites are located at the southern part of the pluton and cover an area of 155 km^2 (Fig. 2A). They consist of K-feldspar (45%–65%), plagioclase (10%–15%) and quartz (25%–30%) with minor amphibole and biotite. The medium-grained syenogranites intruded the coarse-grained syenogranite, and have a total of 78 km^2. They have similar mineral assemblages, including K-feldspar (50%–60%), plagioclase (10%–20%) and quartz (25%–30%) associated with minor amphibole and biotite. The third-stage porphyritic syenogranites in the northern part occurs as stocks with an outcrop area of 56 km^2 (Fig. 2B). They are light gray to pink, and show porphyritic textures. The phenocrysts are mainly 2–5 mm quartz and K-feldspar. K-feldspar is mostly subhedral and perthitic, and generally shows Carlsbad twinning (Fig. 2E). Plagioclase is mainly platy with well-developed polysynthetic twinning. Quartz shows granular shape (Fig. 2E, F). Biotites are partly altered to chlorite (Fig. 2F). Accessory minerals include zircon, apatite, monazite, magnetite, ilmenite, and fluorite.

The Tianqiaogou dioritic pluton, covering an area of 9 km^2 (Fig. 1C), intruded into the early Cretaceous Heyu granitic pluton (148–134 Ma; Gao et al., 2010; N. Li et al., 2012). Rocks from the Tianqiaogou pluton mainly consist of monzodiorite (Fig. 2D) with minor monzonite (Fig. 2C). Monzodiorites are generally grayish black in color with massive structure and subhedral granular texture (Fig. 2H). They are mainly composed of plagioclase (45%–55%), K-feldspar (15%–20%), amphibole (20%–25%), biotite (5%–10%) and quartz (<5%). Plagioclase is weakly sericitized but retains twinning textures. Amphibole is partly replaced by chlorite. Quartz occurs as granular. Monzonite is composed of plagioclase (25%–30%), K-feldspar (30%–35%), amphibole (15%–20%) and biotite (5%–10%) (Fig. 2G). Subhedral to anhedral K-feldspar surrounds subhedral plagioclase. Anhedral to subhedral amphibole is interestingly distributed among plagioclase and k-feldspar grains. Therefore, the monzonites were probably differentiation products of the monzodiorites. The rocks from the Tianqiaogou pluton will be referred to as TQG monzodiorite in the following discussion.

4. Analytical results

4.1. Zircon U–Pb dating

Three samples from the Taishanmiao (TSM) and Tianqiaogou (TQG) plutons were chosen for zircons selecting and LA-ICP-MS U–Pb dating. Analytical methods are given in Supplemental file, and the results are listed in Supplementary Table A1. Representative CL images of the zircons in this study are shown in Fig. 3. The age data are plotted in Fig. 4.

4.1.1. Taishanmiao pluton

Sample TSM-31 (33°51′24″N, 112°09′46″E) is coarse-grained syenogranite. Zircon grains from this sample are transparent and colorless to pale yellow, and show subhedral to euhedral columnar shapes (80–250 μm long) with aspect ratios of 2:1 to 3:1 (Fig. 3). They show clear oscillatory zoning in CL images and have high Th/U ratios ranging from 0.54 to 2.02 (Supplementary Table A1), indicating magmatic origin (Belousova et al., 2002). Among nineteen grains analyzed spots, fourteen analyses yielded $^{206}Pb/^{238}U$ ages varying from 121 Ma to 131 Ma with a weighted mean $^{206}Pb/^{238}U$ age of 125 ± 2 Ma (MSWD = 2.5) (Fig. 4A). One spot (TSM-31-19) considerably deviate from the concordia. Four grains (TSM-31-1, TSM-31-5, TSM-31-6 and TSM-31-8) have old $^{206}Pb/^{238}U$ ages of 144 Ma, 148 Ma, 142 Ma and 1038 Ma (Supplementary Table A1), respectively, probably inherited from country rocks.

Sample TSM-20 is from the medium-grained syenogranite (33°53′38″N, 112°10′26″E). Its zircon grains range in size from 50 to 300 μm long with a length to width ratio of 2:1 to 3:1 (Fig. 3). They also show clear oscillatory zoning in CL images and have high Th/U ratios (0.75 to 2.09; Supplementary Table A1), typical features of magmatic origin (Belousova et al., 2002). Twenty spots of zircons from sample TSM-20 were analyzed. Two grains (TSM-20-01 and TSM-20-13) have $^{206}Pb/^{238}U$ ages of 143 Ma and 142 Ma, respectively, likely inherited zircons. Five spots deviate from the concordia. The remaining thirteen spots have concordant or nearly concordant $^{206}Pb/^{238}U$ ages of 106 to 125 Ma, yielding a weighted mean $^{206}Pb/^{238}U$ age of 115 ± 2 Ma (MSWD = 1.6) (Fig. 4B).

4.1.2. Tianqiaogou pluton

The monzonite sample TQG-1 is from the Tianqiaogou pluton (33°45′56″N, 111°56′6″E). Zircons from this sample are colorless or light-brown, transparent to semi-transparent, and euhedral to subhedral. They range in size from 50 to 200 μm with length to width ratios of 2:1 to 3:1. Some zircon grains show oscillatory growth zoning, the others are homogeneous in CL images (Fig. 3). They have high Th/U ratios (0.44 to 1.22), suggesting a magmatic origin (Belousova et al., 2002). Sixteen analyses yield $^{206}Pb/^{238}U$ ages ranging from 119 Ma to 129 Ma. Except three analyses considerably deviating from the concordia, thirteen analyses are concordia and yield a weighted mean $^{206}Pb/^{238}U$ age of 122 ± 2 Ma (MSWD = 0.8) (Fig. 4C), indicating that the Tianqiaogou pluton emplaced contemporary with the Taishanmiao granitic pluton (Fig. 4D).

4.2. Whole rock major and trace elements

Major and trace element data for the representative samples of the Taishanmiao and Tianqiaogou plutons are listed in Table 1 and the full data set are listed in Supplementary Table A2.

Rocks from the Taishanmiao pluton are rich in silica and alkaline, especially K. They are all subalkaline on the total alkaline vs. silica (TAS) diagram (Fig. 5G). Most samples plot in the high-K calc-alkalic field in the plot of SiO_2–K_2O (Fig. 5H). The rocks are metaluminous to weakly peraluminous with ACNK ratios (molar ratio of $Al_2O_3/(CaO + Na_2O + K_2O)$) of 0.92 to 1.14.

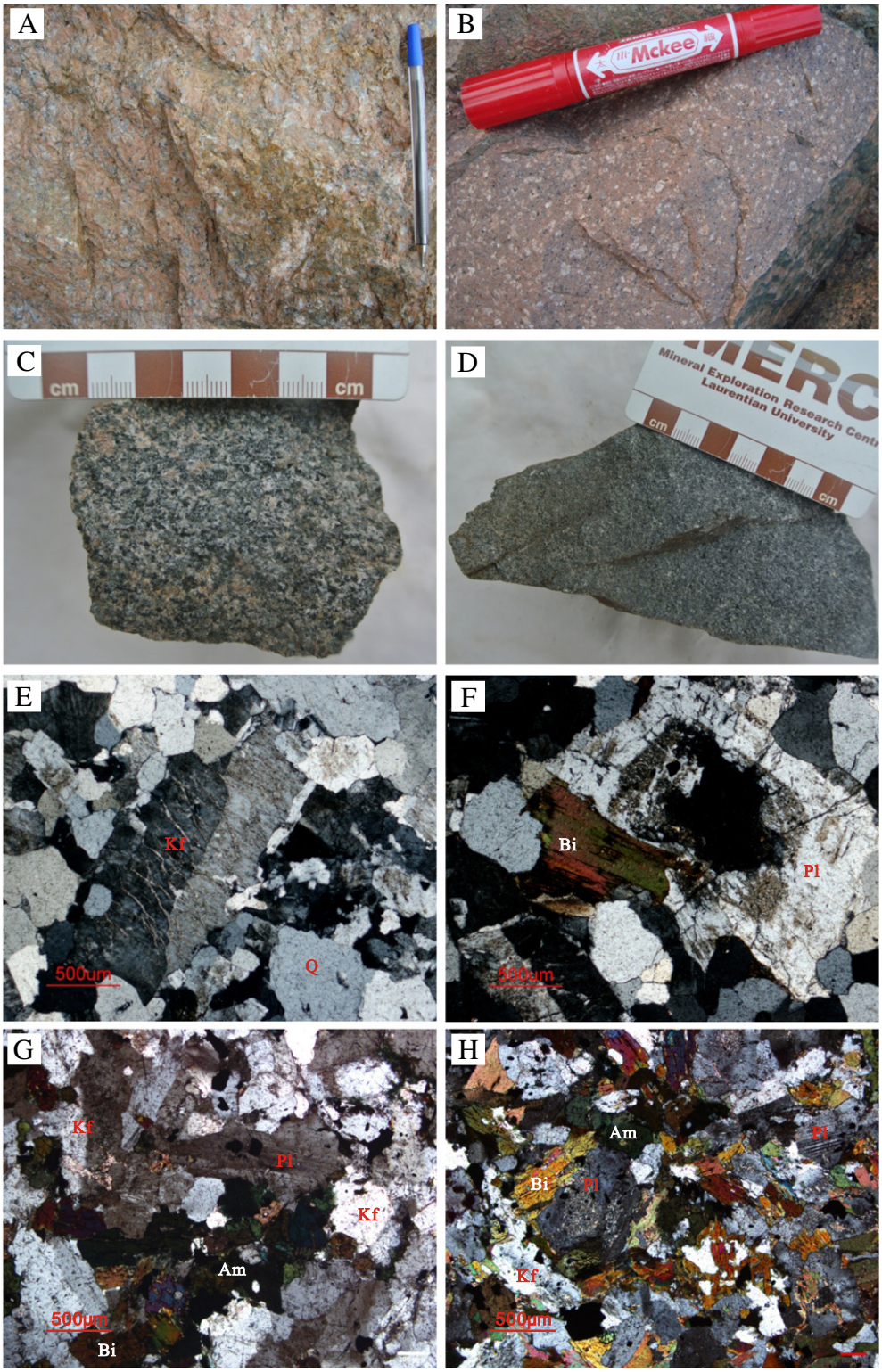

Fig. 2. Field geological observation and petrography: (A) medium–coarse-grained syenogranite of the Taishanmiao pluton. (B) Porphyritic syenogranite of the Taishanmiao pluton. (C) Monzonite of the Tianqiaogou pluton. (D) Monzodiorite of the Tianqiaogou pluton. (E) K-feldspar from the Taishanmiao pluton occurs as subhedral slabs with perthitic textures. (F) Schistose biotite and plagioclase with sericitization in its center in the Taishanmiao pluton. (G) Monzonite of the Tianqiaogou pluton shows monzonitic texture that the k-feldspar forms as subhedral to anhedral crystals and surrounding subhedral plagioclase. (H) Hypidiomorphic granular texture of the Tianqiaogou pluton monzodiorites.

However, rocks from the Tianqiaogou pluton have intermediate composition, and mainly belong to monzodiorite and monzonite in the TAS diagram (Fig. 5G). They have high total Fe_2O_3, MgO, and $Mg^{\#}$ (Supplementary Table A2). They are high-K calc-alkalic to shoshonitic, with total alkali ($K_2O + Na_2O$) contents of 6.5–9.7 wt.% and Na_2O/K_2O ratios of 1.0–2.1 (Fig. 5G). They define linear trend in the Harker diagrams (Fig. 5A–F).

Rocks from the Taishanmiao and Tianqiaogou plutons have chondrite-normalized rare earth element (REE) patterns that are enriched in light REE (Fig. 6A, C). Rocks from the Taishanmiao

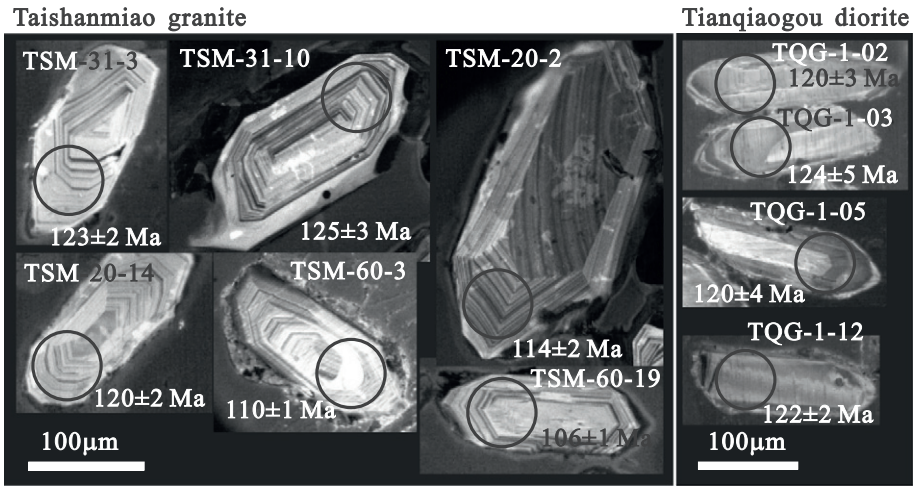

Fig. 3. Representative cathodoluminescence (CL) images of zircon grains from the Taishanmiao and Tianqiaogou plutons. Black circles show the location of LA-ICP-MS U–Pb analyses as well as the LA-MC-ICP–MS Hf analyses.

pluton have moderate to large negative Eu anomalies (Fig. 6A), whereas those from the Tianqiaogou pluton have weak negative Eu anomalies (Fig. 6C).

The rocks from the two plutons also show similar primitive mantle normalized trace element patterns, such as enrichment of large ion lithophile elements (LILE,), and depletion of high field strength elements (HFSE) (Fig. 6B, D).

4.3. Whole rock Sr–Nd isotopes

Whole rock Sr–Nd isotopic data for the Taishanmiao and Tianqiaogou plutons are listed in Table 2. Rocks from the Taishanmiao pluton have initial $^{87}Sr/^{86}Sr$ ratios ranging from 0.7089 to 0.7174 and $\varepsilon_{Nd}(t)$ values from −16.1 to −7.5. Their model Nd ages vary from 1.19 to 2.01 Ga (Table 2).

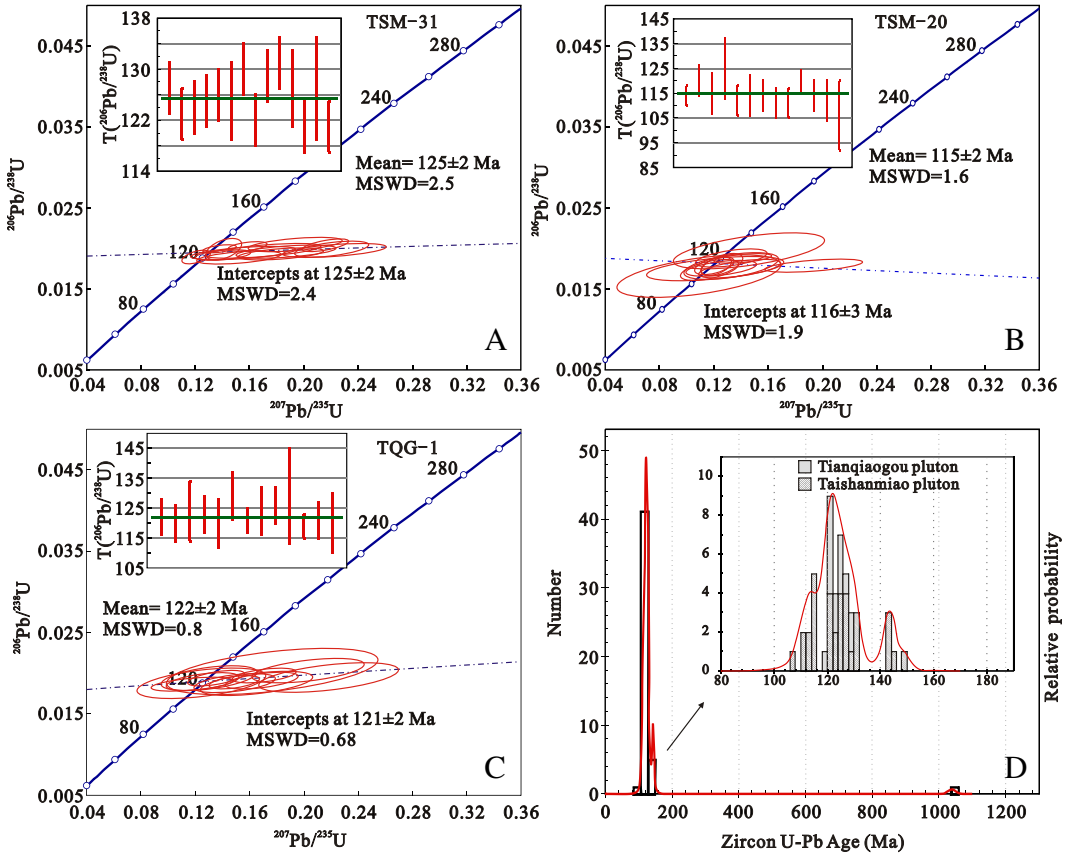

Fig. 4. LA-ICP-MS zircon U–Pb concordant plots of the Taishanmiao and Tianqiaogou plutons.

Table 1
Major (wt.%) and trace element concentrations($\times 10^{-6}$) of the Taishanmiao and Tianqiaogou plutons.

Rock type	Coarse grained syenogranite			Medium grained syenogranite			Porphyritic syenogranite			Monzodiorite		
Intrusion	Taishanmiao			Taishanmiao			Taishanmiao			Tianqiaogou		
Sample no.	Tsm-2	Tsm-5	Tsm-7	Tsm-47	Tsm-50	Tsm-53	Tsm-57	TSM-60	Tsm-1-2	TQG-2	13TQG-4	13TQG-2
SiO_2	72.20	77.24	77.48	77.57	78.12	76.37	73.43	76.81	77.96	52.02	51.73	54.61
TiO_2	0.26	0.08	0.06	0.09	0.09	0.22	0.26	0.15	0.11	2.17	2.06	1.71
Al_2O_3	14.25	12.60	12.05	12.05	11.94	12.34	13.24	12.53	11.96	16.44	17.54	16.37
$Fe_2O_3^T$	2.44	1.01	1.09	1.03	1.10	1.78	1.91	0.83	1.20	11.39	10.82	9.22
MnO	0.04	0.01	0.03	0.02	0.02	0.04	0.20	0.01	0.01	0.17	0.20	0.16
MgO	0.62	0.14	0.13	0.10	0.12	0.36	0.43	0.07	0.15	4.03	2.92	2.66
CaO	1.23	0.48	0.50	0.43	0.50	0.81	1.06	0.39	0.55	5.69	5.43	4.78
Na_2O	4.17	3.65	3.51	4.16	3.62	3.36	4.18	3.80	3.45	4.57	5.12	4.61
K_2O	4.65	4.83	5.21	4.63	4.57	4.73	5.20	4.55	4.66	2.39	2.50	2.89
P_2O_5	0.08	0.01	0.01	0.01	0.01	0.04	0.06	0.01	0.02	0.61	0.97	0.83
LOI	0.64	0.57	0.83	0.58	0.54	0.6	1.37	0.54	0.60	0.74	0.90	1.57
Total	99.94	100.06	100.07	100.08	100.08	100.04	99.99	99.69	100.08	99.48	100.19	99.41
$Mg^{\#}$	33.5	21.5	19.1	16.1	17.8	28.6	30.8	14.3	19.8	41.2	34.8	36.3
Ga	23.8	21.3	17.0	20.1	20.5	18.0	18.1	25.4	20.6	20.3	22.7	20.5
Cs	2.05	3.14	1.20	3.04	3.92	1.75	2.58	0.85	1.24	1.10	0.71	1.00
Rb	161	226	153	240	258	142	161	293	200	79.6	50.3	60.2
Ba	1531	13.1	43.1	7.19	17.3	113	588	16.0	13.4	1097	1154	1551
Th	38.1	10.9	4.64	22.2	26.7	16.4	17.5	78.5	23.4	4.47	3.73	6.35
U	15.1	2.66	1.90	4.54	9.17	3.06	5.76	6.48	5.20	0.91	0.75	0.95
Nb	45.9	71.5	13.2	69.1	87.1	34.2	32.0	76.3	59.9	31.2	44.9	37.7
Ta	2.74	6.88	1.37	5.18	8.73	2.94	3.12	6.73	6.07	2.05	2.14	2.05
Sr	380	3.28	5.68	2.01	4.16	28.8	74.3	8.89	3.60	721	768	746
Y	8.90	2.60	1.21	6.20	7.11	6.16	5.61	35.1	2.83	32.9	40.1	37.3
Zr	157	100	115	164	172	97.3	149	169	152	44.0	243	249
Hf	4.80	5.6	4.63	7.16	8.28	3.70	5.05	6.50	6.79	1.33	5.11	5.25
La	52.6	12.0	5.68	8.71	12.5	11.8	15.6	36.0	17.8	42.4	65.6	64.8
Ce	92.5	28.3	15.8	19.3	27.2	25.4	31.7	68.4	34.9	87.6	134	127
Pr	9.09	2.54	1.00	1.68	2.63	2.92	3.80	6.97	2.96	10.1	16.6	15.4
Nd	29.1	7.14	2.93	4.65	7.57	9.68	13.2	21.2	7.58	40.9	64.6	57.1
Sm	4.20	0.98	0.38	0.77	1.21	1.70	2.37	3.97	0.87	8.44	12.3	10.9
Eu	0.83	0.03	0.04	0.03	0.04	0.18	0.26	0.15	0.05	2.39	3.04	2.88
Gd	2.66	0.67	0.31	0.64	0.95	1.20	1.75	2.96	0.66	6.68	10.6	9.43
Tb	0.35	0.08	0.04	0.14	0.18	0.22	0.25	0.64	0.09	1.07	1.52	1.41
Dy	1.70	0.46	0.21	1.05	1.10	1.33	1.37	4.50	0.51	6.68	8.52	7.90
Ho	0.32	0.10	0.05	0.26	0.31	0.28	0.28	1.02	0.11	1.22	1.61	1.54
Er	0.90	0.33	0.16	1.07	1.09	0.98	0.79	3.36	0.41	3.45	4.19	4.05
Tm	0.14	0.07	0.03	0.21	0.22	0.16	0.13	0.63	0.09	0.49	0.58	0.55
Yb	0.91	0.56	0.21	1.59	1.84	1.09	0.89	4.39	0.81	2.97	3.62	3.27
Lu	0.14	0.10	0.04	0.27	0.32	0.17	0.15	0.66	0.14	0.43	0.55	0.49

$Mg^{\#} = Mg^{2+} / (Mg^{2+} + Fe^{2+}) \times 100$.

Compared with the rocks from the Taishanmiao pluton, rocks from the Tianqiaogou pluton have relatively low initial $^{87}Sr/^{86}Sr$ ratios (0.7054–0.7065) and high $\varepsilon_{Nd}(t)$ (−6.2 to −1.3) values with T_{DM} ages of 1.14−1.50 Ga (Table 2).

4.4. In situ zircon Lu–Hf isotopic compositions

In situ zircon Hf data for the Taishanmiao and Tianqiaogou plutons are listed in Supplementary Table A3 and plotted in Fig. 7B. Zircon grains from the two samples TSM-31 and TSM-20 of the Taishanmiao pluton have variable $\varepsilon_{Hf}(t)$ values (−20.9 to −6.1). Their single-stage model ages (T_{DM}) range from 1037 Ma to 1597 Ma and two stage model ages (*T*C DM) from 1565 Ma to 2490 Ma (Fig. 7B). One inherited zircon grain (t = 1038 Ma) has strong negative $\varepsilon_{Hf}(t)$ values (−19.3) and Archean two-stage model age (3109 Ma). However, zircon grains from sample TQG-1 of the Tianqiaogou pluton have positive $\varepsilon_{Hf}(t)$ values (+2.9 to +6.2) values. They also have younger single-stage model ages (T_{DM} = 556–685 Ma) and two-stage model ages (*T*C DM = 783 Ma–998 Ma) (Table A3; Fig. 7B).

5. Discussion

Although the Taishanmiao and Tianqiaogou plutons have similar zircon U–Pb ages, they have different elemental and isotopic compositions, indicating that they were probably derived from different sources and have different petrogenesis. The genetic relationships between the two plutons have important implications for the tectonic evolution of the southern margin of the NCC during the early Cretaceous.

5.1. Petrogenesis of the Tianqiaogou monzodiorites

5.1.1. Fractional crystallization and accumulation

The TQG monzodiorites have high MgO, MnO, and CaO and total Fe_2O_3 at intermediate SiO_2 contents (Table A2; Fig. 5A–F) and high positive zircon $\varepsilon_{Hf}(t)$ value, significantly different from the crustal-derived melts that generally have low Fe_2O_3 and MgO and negative zircon $\varepsilon_{Hf}(t)$ value (Rudnick and Gao, 2003), suggesting that their parental magmas were derived from the mantle source.

The TQG monzodiorites have variable major and trace element compositions, suggesting that their parental magmas may have experienced varying degrees of fractional crystallization and crystal accumulation. All rocks form negative correlations for MgO, CaO and total Fe_2O_3 against SiO_2 (Fig. 5A, B, E) and positive correlations of Na_2O and K_2O against SiO_2 (Fig. 5G, H), consistent with fractionation of pyroxene, amphibole and plagioclase. Their low $Mg^{\#}$ (32.7–41.2) values indicate that the magma might have experienced fractionation of pyroxene. This fractionation is also

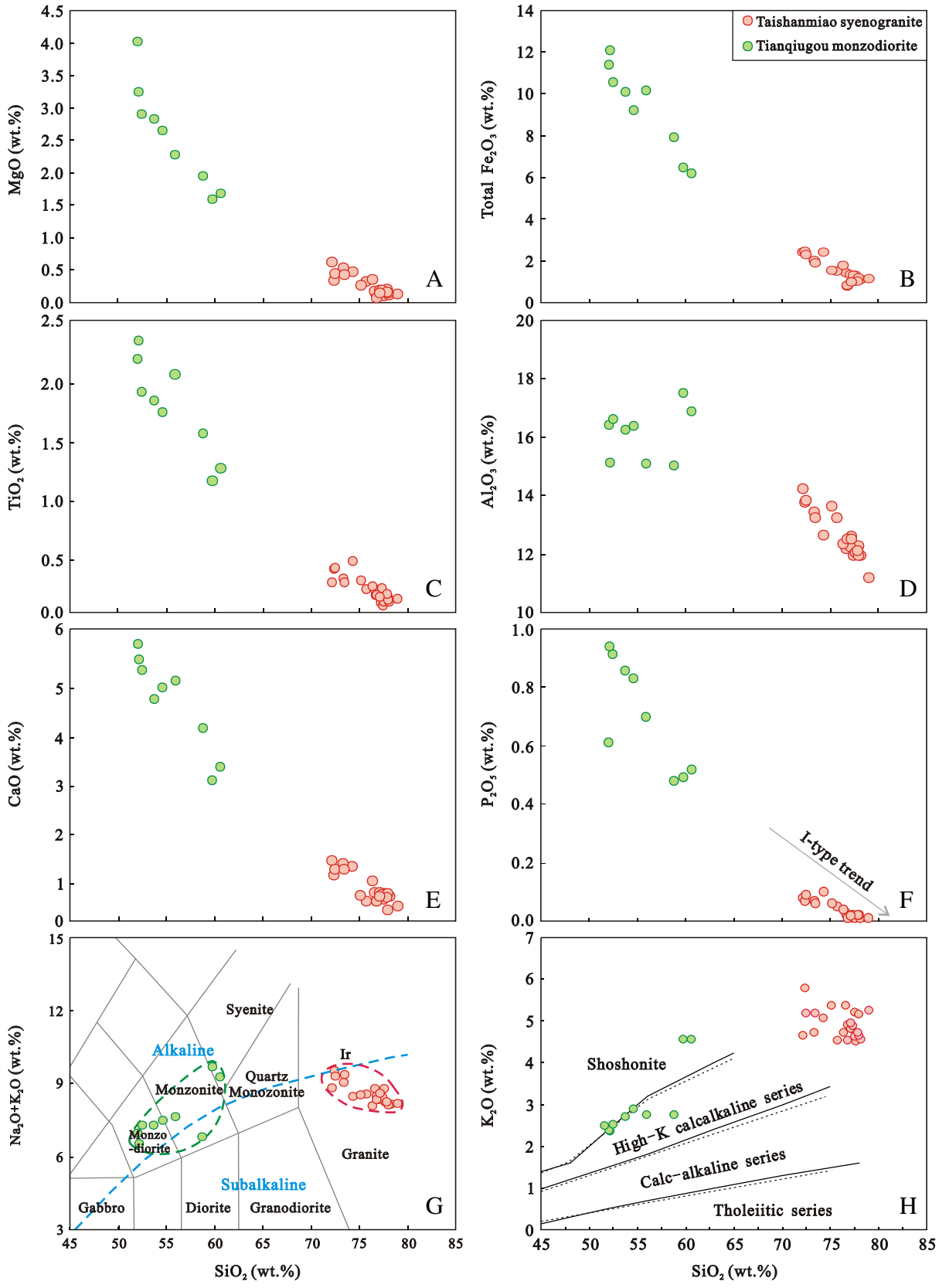

Fig. 5. Major oxides vs. SiO_2 diagram of the Taishanmiao and Tianqiaogou plutons. From Le Maitre et al. (1989).

evidenced by the negative correlations of MgO and Fe_2O_3 against SiO_2 (Fig. 5A, B). Apatite and Fe–Ti oxide fractionations may have also been involved as evidenced by the negative correlation of P_2O_5 and TiO_2 with SiO_2 (Fig. 5C, F). Plagioclase fractionation may not have played an important role as evidenced by slightly positive Eu anomalies (Fig. 6C).

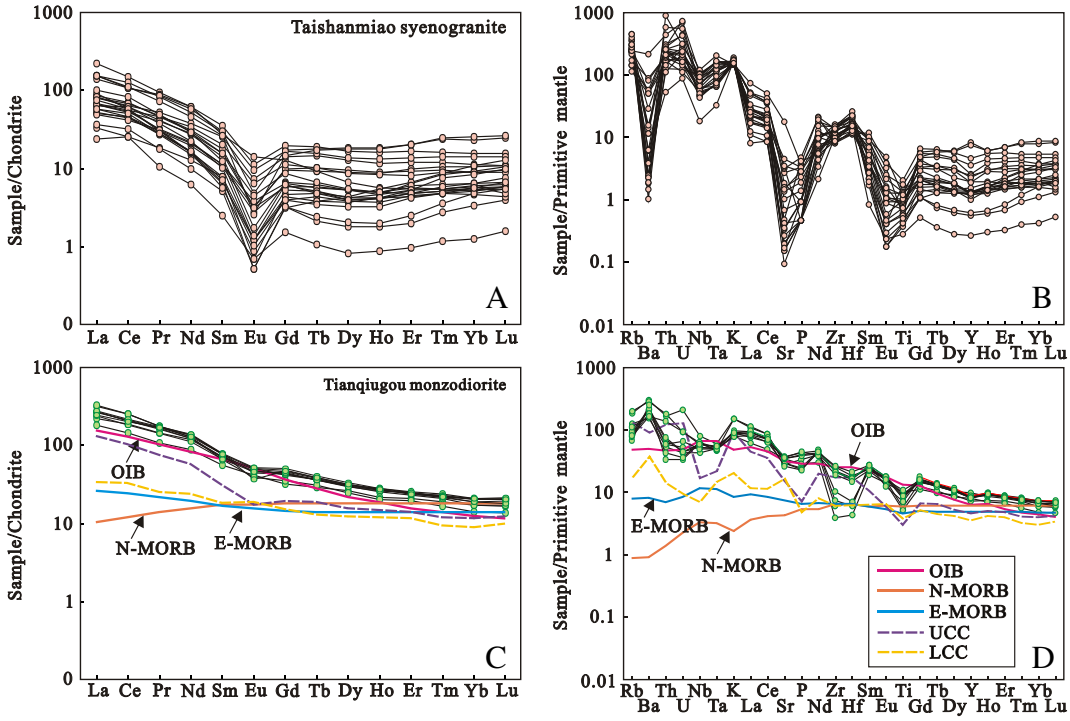

Fig. 6. Chondrite-normalized REE patterns and primitive mantle-normalized incompatible element spider diagrams for the Taishanmiao and Tianqiaogou plutons. The normalization values are from Sun and McDonough (1989).

5.1.2. Crustal contamination

Crustal contamination is almost inevitable for mantle-derived melts during their ascent through continental crust or in the magma chamber (e.g., Castillo et al., 1999). Given that crustal materials generally have low $\varepsilon_{Nd}(t)$, MgO, low $(Nb/Th)_{PM}$ and high $^{87}Sr/^{86}Sr$ ratios (Rudnick and Fountain, 1995), any crustal contamination would have increased I_{Sr} and decreased $\varepsilon_{Nd}(t)$ values of the magmas (Rogers et al., 2000). The TQG monzodiorites show crustal-like elemental characteristics, such as enrichment of LILEs and LREEs and depletion of Nb–Ta (Fig. 6D). They also have highly variable Nd ($\varepsilon_{Nd}(t) = -6.2$ to -1.3) and Sr isotopic values ($I_{Sr} = 0.7054$–0.7065) that cannot be explained by fractionation crystallization alone (Fig. 7A). This geochemical evidence suggests that crustal-derived materials must have been involved in their petrogenesis (e.g. Elburg, 1996; Griffin et al., 2002).

$(Nb/Th)_{PM}$ and $(Th/Yb)_{PM}$ ratios are sensitive to crustal contamination (Rudnick and Fountain, 1995). The TQG monzodiorites have very low $(Nb/Th)_{PM}$ ratios and high $(Th/Yb)_{PM}$ ratios, consistent with variable degrees of crustal contamination (Fig. 8). Crustal contamination could also result in linear correlation for I_{Sr} and $\varepsilon_{Nd}(t)$ against SiO_2. The TQG monzodiorites' positive correlation of SiO_2 vs. I_{Sr}, and negative correlation of SiO_2 vs. $\varepsilon_{Nd}(t)$ (Fig. 9A, B), indicate that their large variable geochemical compositions did not result from simple differentiation, but from crustal contamination. Modeling of crustal contamination processes shows that approximately 20–30% of the amphibolite of the Taihua Group was probably involved in the contamination of mantle-derived basaltic magma (Fig. 7A). Such voluminous contamination led to a dramatic change in the major and trace element compositions (Fig. 5).

Table 2
Whole-rock Sr–Nd isotopic compositions of the Taishanmiao and Tianqiaogou plutons.

Lithology	Sample	$^{87}Rb/^{86}Sr$	$^{87}Sr/^{86}Sr$	2σ	I_{Sr}	$^{147}Sm/^{144}Nd$	$^{143}Nd/^{144}Nd$	2σ	$\varepsilon_{Nd}(t)$	T_{DM} (Ga)	$f_{Sm/Nd}$
Syenogranite	TSM-2	1.1967	0.710996	0.000020	0.7089	0.0916	0.511727	0.000007	−16.1	1.77	−0.53
	TSM-20	21.2383	0.752127	0.000018	0.7174	0.1137	0.511921	0.000007	−12.8	1.87	−0.42
	TSM-38	3.1571	0.715564	0.000019	0.7100	0.1175	0.511897	0.000008	−13.2	1.98	−0.40
	TSM-57	6.1205	0.719604	0.000014	0.7097	0.1139	0.512172	0.000008	−7.9	1.49	−0.42
	TSM-1-2					0.0728	0.511913	0.000006	−12.3	1.34	−0.63
	TSM-5					0.0871	0.512164	0.000006	−7.5	1.19	−0.56
	TSM-7					0.0823	0.511947	0.000008	−11.7	1.40	−0.58
	TSM-21					0.1256	0.512055	0.000009	−10.2	1.89	−0.36
	TSM-60					0.1188	0.511897	0.000007	−13.3	2.01	−0.40
Monzodiorite	TQG-1	0.2570	0.706551	0.000018	0.7061	0.1248	0.512437	0.000007	−2.8	1.22	−0.37
	TQG-2	0.3118	0.705898	0.000018	0.7054	0.1310	0.512518	0.000008	−1.3	1.17	−0.33
	TQG-6	0.5827	0.707498	0.000016	0.7065	0.1062	0.512249	0.000008	−6.2	1.28	−0.46
	13TQG-1	0.2101	0.706267	0.000006	0.7059	0.1163	0.512422	0.000004	−2.9	1.14	−0.41
	13TQG-2	0.2278	0.706024	0.000007	0.7056	0.1210	0.512409	0.000004	−3.3	1.22	−0.39
	13TQG-3	0.1558	0.705904	0.000006	0.7056	0.1193	0.512392	0.000005	−3.6	1.23	−0.39
	13TQG-4	0.1847	0.705944	0.000004	0.7056	0.1206	0.512415	0.000007	−3.2	1.20	−0.39
	13TQG-5	0.1925	0.706013	0.000006	0.7057	0.1248	0.512477	0.000004	−2.0	1.16	−0.37
	13TQG-6	0.3711	0.706890	0.000006	0.7062	0.1233	0.512261	0.000004	−6.2	1.50	−0.37

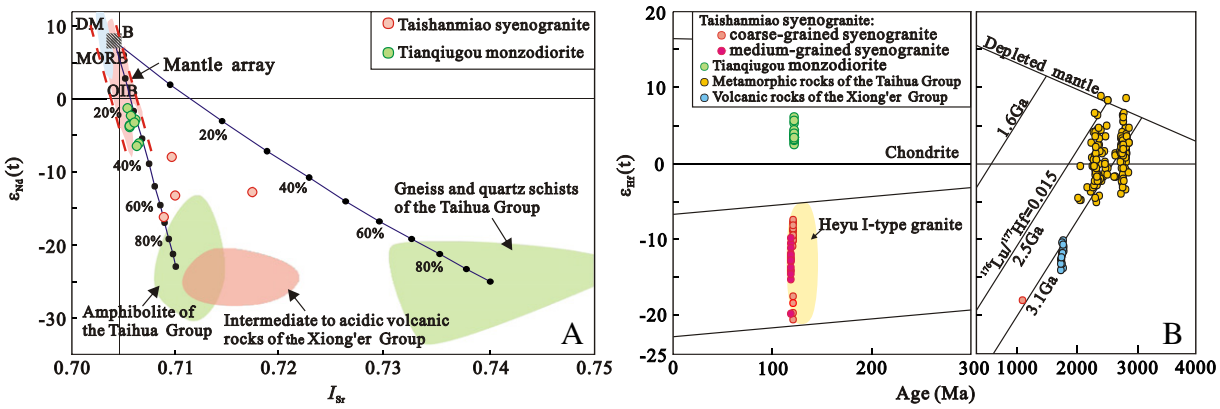

Fig. 7. (A) $\varepsilon_{Nd}(t)$ vs. I_{Sr} and (B) $\varepsilon_{Hf}(t)$ vs. age diagrams of the Taishanmiao and Tianqiaogou plutons. (A) Mixing calculations for source and melt contaminations of the Taishanmiao and Tianqiaogou pluton are shown in the diagrams. The $\varepsilon_{Nd}(t)$ and I_{Sr} values of the amphibolite and gneiss and quartz schists of the Taihua and intermediate to acidic volcanic rocks of the Xiong'er Group are calculated at $t = 120$ Ma. The mixing parameters used are: Amphibolite of Taihua Group: $Sr = 388 \times 10^{-6}$, $I_{Sr} = 0.71$, $Nd = 27 \times 10^{-6}$, $\varepsilon_{Nd}(t = 120) = -23$ (Huang and Wu, 1990; Ni et al., 2012); gneiss and quartz schists of the Taihua Group: $Sr = 322 \times 10^{-6}$, $I_{Sr} = 0.74$, $Nd = 30 \times 10^{-6}$, $\varepsilon_{Nd}(t = 120) = -25$ (Huang and Wu, 1990); and mantle-derived basaltic magma (B): $Sr = 150 \times 10^{-6}$, $I_{Sr} = 0.704$, $Nd = 15 \times 10^{-6}$, $\varepsilon_{Nd} = 8$ (Jahn et al., 1999). Other data sources: intermediate to acidic volcanic rocks of the Xiong'er Group are from He et al. (2010), Peng et al. (2008) and Wang et al. (2010); DM (depleted mantle) and mantle array are after Hart and Zindler (1986); and OIB and MORB data are from Sun and McDonough (1989). (B): Data source of the Heyu granitic pluton: Gao et al. (2010); data source of the Neoarchean metamorphic rocks of the Taihua Group: Diwu et al. (2010) and Liu et al. (2009); data source of the Paleoproterozoic metamorphic rocks of the Taihua Group: Diwu et al. (2007) and X.S. Xu et al. (2009); and data source of the volcanic rocks of the Xiong'er Group: Wang et al. (2010).

5.1.3. Nature of the mantle source

The TQG monzodiorites have variable SiO_2, MgO, I_{Sr}, $\varepsilon_{Nd}(t)$ and $\varepsilon_{Hf}(t)$ values (Figs. 5A, 7). These geochemical features indicate that none of the samples represent primary magma compositions. In the $\varepsilon_{Nd}(t)$ vs. I_{Sr} diagrams (Fig. 7A), the TQG monzodiorites form a relatively narrow field and plot along the mantle array. They define a mixing line between the mafic end-member with low I_{Sr} (<0.7054) and high $\varepsilon_{Nd}(t)$ (>−1.3) and $\varepsilon_{Hf}(t)$ (>+6.2) values and the crustal end-member with high I_{Sr} (>0.7065) and negative $\varepsilon_{Nd}(t)$ (<−6.2) values. They also have relatively high total Fe_2O_3 (>11.4 wt.%) and TiO_2 (>2.33 wt.%) concentrations (Table A2), indicating that their parental magmas were enriched in Fe and Ti. These geochemical features are similar to those of experimental melts from the fertile peridotite (Falloon et al., 1988; Hirose and Kushiro, 1993). Their Sr–Nd isotopic compositions are slightly enriched relative to OIB and MORB-like magmas, but distinct depleted relative to the Mesozoic mafic igneous rocks from the NCC that were derived from partial melting of an enriched lithospheric mantle (Zhang et al., 2013). In addition, they have relatively high positive $\varepsilon_{Hf}(t)$ values (up to 6.2), indicating that they were derived from a relatively juvenile lithospheric mantle source (Fig. 7B).

The TQG monzodiorites show negative $\varepsilon_{Nd}(t)$ and positive $\varepsilon_{Hf}(t)$ values, indicating decoupling of the Lu–Hf and Sm–Nd isotopic systems. In general, Hf has a low solubility in aqueous fluids and is effectively transported into the mantle wedge by fluids derived from the subducted sediment or crust. In contrast, Nd is more mobile in both aqueous fluids and melts (Pearce et al., 1999). Their different isotopic behaviors lead to significant decoupling of Hf–Nd that yield radiogenic high ε_{Hf} compared with unradiogenic low ε_{Nd} (Patchett et al., 1984; Vervoort et al., 1999). The Hf–Nd decoupling of the TQG monzodiorites indicates that their mantle source may have been modified by fluids released from the subducted marine sediment or oceanic crust. This process would also lead to depletion of their HFSE (Fig. 6B, D).

5.2. Origin of the Taishanmiao syenogranites

5.2.1. Genetic type

Most TSM syenogranites are metaluminous to slightly peraluminous with A/CNK < 1.1 and A/NK > 1.0. Apatite can reach saturation in metaluminous and mildly peraluminous magmas (A/CNK < 1.1), but is highly soluble in strongly peraluminous melts (Wolf and London, 1994). The negative correlation between P_2O_5 and SiO_2 thus indicates

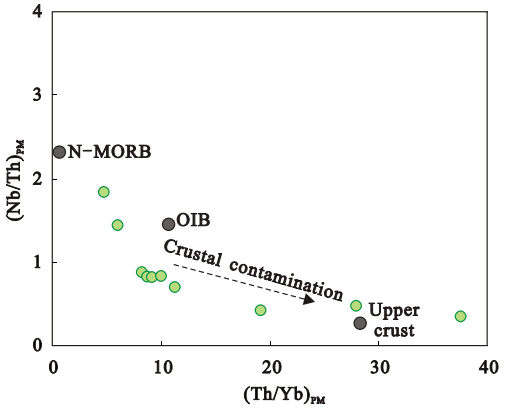

Fig. 8. Plots of $(Th/Yb)_{PM}$ versus $(Nb/Th)_{PM}$ ratios of rocks from the Tianqiaogou pluton. Data for N-MORB and OIB are from Sun and McDonough (1989); data for upper crust are from Gao et al. (1998).

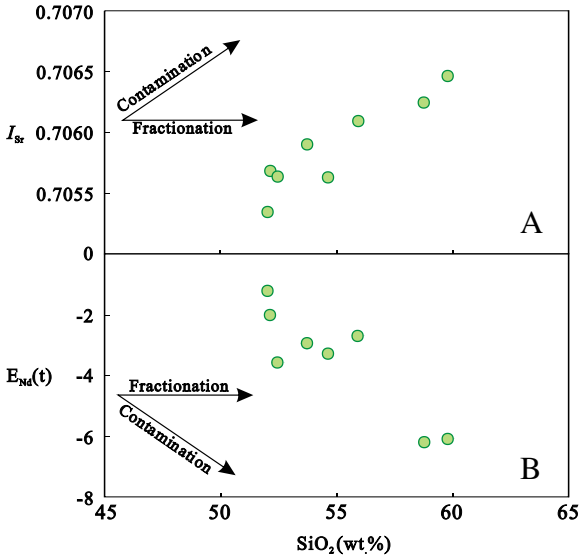

Fig. 9. Diagrams of I_{Sr} and $\varepsilon_{Nd}(t)$ versus SiO_2 for the Tianqiaogou pluton show that the crustal contamination is a dominant factor to form the TQG monzodiorite. The arrows are each consistent with the array of contamination or fractionation processes.

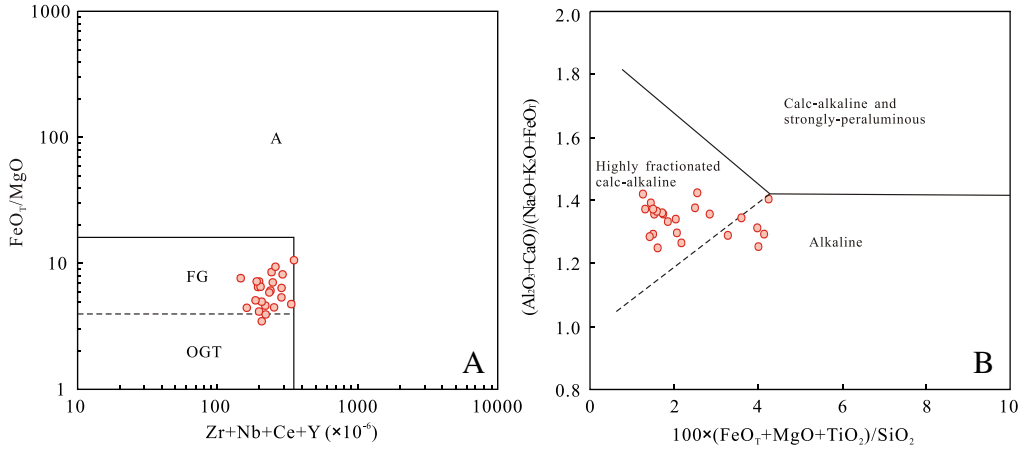

Fig. 10. Chemical discrimination diagrams for the Taishanmiao pluton (after Whalen et al., 1987; Sylvester, 1998) (A): A—A-type granite, FG—Fractionated felsic granites, OGT—unfractionated M-, I- and S-type granites.

that the TSM syenogranites are I-type granites (Fig. 5F; Chappell, 1999; Li et al., 2007; Wu et al., 2003).

Previous studies classify the rocks from the Taishanmiao pluton as A-type granites (Ye et al., 2008). However, it is difficult to distinguish high-Si aluminous A-type granite ($SiO_2 > 72$ wt.%) from highly differentiated I-type granites due to their similar mineralogy and geochemistry when the magmas approach the low-eutectic point (Li et al., 2007). In the FeO_T/MgO vs. (Zr + Nb + Ce + Y) diagrams (Fig. 10A), the Taishanmiao syenogranites plot into the fractionated granite field. In addition, they have lower FeO_T/MgO ratios than that of A-type granites (Whalen et al., 1987). Their zircon saturation temperatures range from 734 °C to 799 °C (Watson and Harrison, 1983), lower than those of A-type granite (King et al., 2001). In addition, most samples fall into the highly fractionated calc-alkaline field in Fig. 10B. Thus, the TSM syenogranites belong to the highly fractionated I-type, rather than the aluminous A-type granites.

5.2.2. Petrogenesis

Markedly peraluminous granitoids could be generated by partial melting of the lower crust or fractional crystallization of mafic magmas (Zhao et al., 2013a,b; Zhou et al., 2013). The TSM syenogranites have high SiO_2, low MgO content, negative $\varepsilon_{Nd}(t)$ and $\varepsilon_{Hf}(t)$ values (Figs. 5A, 7), suggesting a crustal origin. Magmatic zircons from the TSM syenogranites show Mesoproterozoic to Paleoproterozoic Hf two-stage model ages, demonstrating that the syenogranites were partial melts of the recycled ancient continental crust, rather than produced by fractional crystallization of mafic magmas. Their widely variable zircon Hf isotopes suggest a heterogeneous source region (e.g. Zhao et al., 2013a).

The oldest basement rocks in the southern margin of the NCC are from the Taihua Group that consists of amphibolite and granulite facies metamorphic rocks. The protoliths of the Taihua Group were formed in the Neoarchean and Paleoproterozoic (2.84–2.26 Ga) and were strongly deformed and metamorphosed at 2.1–1.8 Ga (Kröner et al., 1988; Wan et al., 2006; X.S. Xu et al., 2009). Another widespread lithologic unit in the region is the Xiong'er Group that formed at 1.75 to 1.80 Ga (Zhao et al., 2004). The TSM syenogranite has similar initial $^{87}Sr/^{86}Sr$ values to those of the amphibolites of the Taihua Group at 120 Ma (Ni et al., 2012; X.S. Xu et al., 2009) and those of the volcanic rocks from the Xiong'er Group (He et al., 2010; Peng et al., 2008; Wang et al., 2010), but lower than those of the gneiss and quartz schists from the Taihua Group (Huang and Wu, 1990) (Fig. 7A). Their $\varepsilon_{Nd}(t)$ values are also close to those of the amphibolite of the Taihua Group, but obviously higher than those of gneiss and quartz schists of the Taihua Group and volcanic rocks of the Xiong' Group (Fig. 7A). Based on the isotopic compositions and model ages, the metamorphic basement rocks from the Taihua Group were probably the dominant source rocks for the TSM syenogranites. However, some zircons have Hf two-stage model ages (1.6–2.5 Ga) that are much younger than the age of the Taihua Groups. In addition, their $\varepsilon_{Hf}(t)$ values are also higher than those of the rocks from the Taihua Group at t = 120 Ma (Fig. 7B). This evidence suggests that melting of the Taihua metamorphic basement rocks alone cannot produce the parental magma of the Taishanmiao pluton. The mantle-derived mafic melts with more depleted Hf and Nd isotopic compositions are likely to have been involved in their petrogenesis.

The TQG monzodiorites have obviously high $\varepsilon_{Hf}(t)$ values (+2.9 to +6.1) and $\varepsilon_{Nd}(t)$ values (−6.2 to −1.3) (Fig. 7A, B), and were derived from the juvenile lithospheric mantle beneath the NCC as discussed above. A mixing model between the mantle and the lower crust-derived magma is applied (Fig. 7A), together with fractional crystallization is used to constrain the processes. Simple modeling of source mixing indicates that mixing between the metamorphic rocks (amphibolite, gneiss and quartz schists of the Taihua Groups) and the mantle-derived melts with ratios of 3/7 to 6/4 could explain the Sr–Nd isotopic compositions of the TSM syenogranites.

Depletion of Ba, Nb, Sr, P, Ti and Eu of the highly fractionated I-type granites from the TSM syenogranites is consistent with extensive fractional crystallization (Fig. 6B; Chappell, 1999). Negative Nb, Ta and Ti anomalies are considered to have resulted from fractionation of Ti-bearing phases, and negative P anomalies from apatite separation. Fractionation of biotite and hornblende may explain the negative correlation of MgO and Fe_2O_3 with SiO_2 (Fig. 5A, B). Eu depletion requires extensive fractionation of plagioclase and/or K-feldspar. Sr decreases quickly with decreasing Ba and Rb (Fig. 11A, B), indicating separation of plagioclase and K-feldspar. The TSM syenogranites have low REE and enrichment of HREE (e.g., Y and Yb), suggesting lack of garnet as a residual mineral at shallow depths (Martin, 1999), and in marked contrast to an adakitic granite rich in Sr and poor in Y (Defant and Drummond, 1990; Xiong et al., 2005).

5.3. Implications for tectonic evolution

Zhang et al. (1996) proposed that continental collision between the North China craton (NCC) and the Yangtze Craton (YZC) in Qinling Orogenic Belt occurred during the early Mesozoic (ca. 245–235 Ma) with an intracontinental subduction in the early stage of collision (Fig. 12A). At this time, the lithosphere was markedly compressed, shortened and thickened, which resulted in the Luonan–Luanchuan overthrust system on the southern margin of the NCC (Fig. 12A) (Zhang et al., 1996). The Mesozoic lower crust mafic xenoliths (~160 Ma) from Xinyang, Henan Province, southern margin of the NCC, indicate that the Mesozoic lower crust extended to at least 41–56 km depth (Zheng et al., 2003).

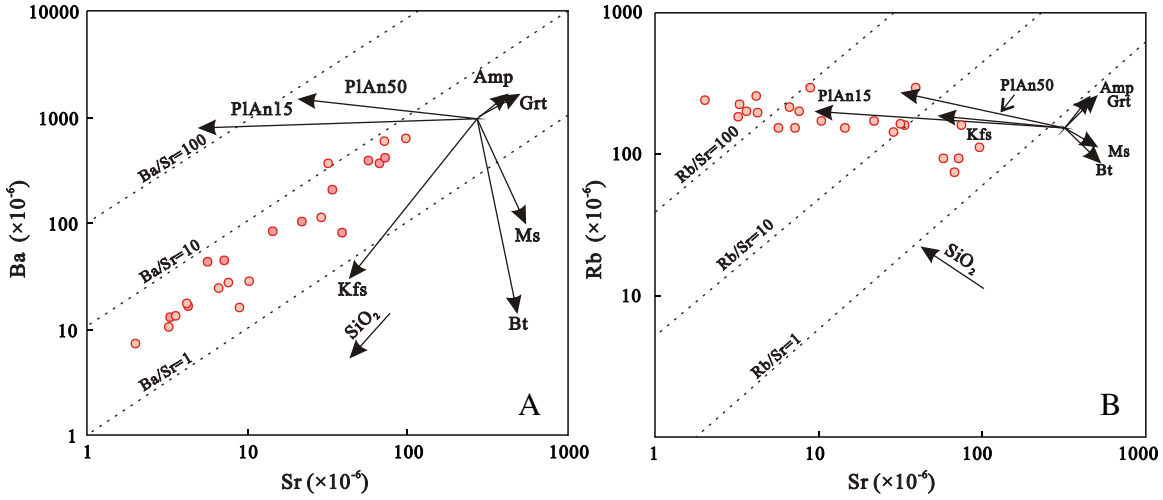

Fig. 11. (A) Ba vs. Sr and (B) Rb vs. Sr diagrams of the Taishanmiao pluton show that fractionation of plagioclase and K-feldspar plays an important role in the differentiation. Trends on these diagrams correspond to up to 50% fractionation crystallization of the main rock-forming minerals (after Janoušek et al., 2004; Li et al., 2007). The dashed lines represent the Ba/Sr and Rb/Sr ratios. Pl_{An50}—plagioclase (An = 50); Pl_{An15}—plagioclase (An = 15); Kfs—K-feldspar; Bi—biotite; Ms—muscovite; Grt—garnet; Amp—amphibole.

The widespread late Jurassic to early Cretaceous adakitic granites (ca. 160–135 Ma) in the southern margin of the NCC form a roughly northwest–southeast-trending belt, also implying formation of the thickened crust before late Jurassic (Fig. 12B; Gao et al., 2010; Li et al., 2012b; Mao et al., 2010; Zhao et al., 2012).

In the Waifangshan area, the 148–135 Ma Heyu adakitic pluton marks the transformation of the lithosphere from thickening to thinning in the southern margin of the NCC (Gao et al., 2010; Li et al., 2012b). During this time, the regional tectonic regime changed to an extensional setting. The overthickened lithosphere underwent extensional thinning that triggered further asthenospheric upwelling, mafic magma underplating, and melting of the middle-lower crust (Fig. 12B) (Mao et al., 2010; Wu et al., 2005). The voluminous felsic magma emplaced along the Luanchuan fault belt and generated the peraluminous granites, such as the monzogranite in the Xiong'er and Taihua Groups (Fig. 12B).

The 124–114 Ma highly fractionated I-type TSM syenogranites are geochemically different from the adakitic granites, and were formed under lower pressure conditions due to intense intracontinental extension and lithospheric thinning (Fig. 12C). In the NCC, eclogite xenoliths inform the Cenozoic basalts and the high pressure granulites do not contain garnet, also implying that Cenozoic lithosphere was much thinner than in the Mesozoic; up to 10 km lowermost crust was delaminated (Zheng et al., 2003). These lines of evidence suggest that crustal thinning occurred during the Mesozoic and Cenozoic, and the southern margin of the NCC may have been transformed into an extensional intraplate environment before 125 Ma (Fig. 12C).

The identification of the magma mixing in the TSM syenogranites reflects significant mantle–crust interaction in the early Cretaceous in the southern margin of the NCC. The underplated basaltic magma may have supplied both energy and materials for the generation of the granitoids. Simultaneously, the mantle derived mafic magma underwent crustal contamination during their ascent to the continental crust and formed the TQG monzodiorites.

The evolution from the adakitic to highly fractionated I-type granitoids and generation of the mantle derived dioritic plutons indicate the progressive lithospheric thinning and the transformation of the tectonic regime to an intensive extensional setting in the early Cretaceous at the southern margin of the NCC.

During the Early Cretaceous (160–110 Ma), intensive mafic to felsic magmatism, large-scale Au and Mo mineralization, voluminous metamorphic complex and extensional basins occurred not only in the southern margin of the NCC, but also in Jiaodong Peninsula, Taihang, Luxi, and Liaodong areas (Goldfarb and Santosh, 2014; Guo et al., 2013; Tang et al., 2013; Yang et al., 2014; Zhai and Santosh, 2013; Zhang, 2012; Zhang et al., 2013), suggesting that these processes were controlled by a common geodynamic mechanism rather than by different independent tectonic events. The late Mesozoic concurrent compressional–extensional structures, tectonic reactivation, lithospheric thinning and craton destruction of the eastern NCC coincide in time with a significant increase in the growth rate and a large change in the subduction direction of the Pacific plate (Bartolini and Larson, 2001; Sun et al., 2007). Consequently, more and more investigations have suggested that the lithospheric extension and thinning of the NCC were triggered by the long-term westward subduction of the Paleo-Pacific plate beneath the east Asian continental margin (Goldfarb and Santosh, 2014; Guo et al., 2013; Tang et al., 2013; Zhao et al., 2007; Zhu et al., 2010, 2012). The flat-slab subduction of the Paleo-Pacific plate probably reached as far as ~1300 km towards the interior of the continent and resulted in widespread late Mesozoic magmatism (Li and Li, 2007). In addition, subduction may have exerted a stronger influence on the east than the western part of the NCC, consistent with the phenomenon that widespread late Mesozoic granitic plutons are in the eastern Qinling Orogenic Belt but not in the western Qinling Orogenic Belt. These events also provided subducted-slab-derived fluids/melts that significantly modified the geochemical composition and geophysical characteristics of the lithospheric mantle, as indicated by the decoupling of the Nd–Hf isotope of the TQG monzodiorites. Subsequently, the asthenospheric upwelling and lithospheric thinning may occurred mainly along major rupture zones that penetrated the lithospheric mantle along the margins of the NCC (Cai et al., 2013; Ma et al., 2014; Tian and Zhao, 2011; Yang et al., 2012). The influence of the long-distance subduction of the Paleo-Pacific plate has possibly reached to the Xiong'er-Xiaoqinling regions in the interior of the continent Asia (Li et al., 2012a).

6. Conclusions

The 122 Ma Tianqiaogou monzodiorites were produced by partial melting of relatively juvenile lithospheric mantle beneath the NCC and underwent crustal contamination during their ascent. The 115–125 Ma Taishanmiao syenogranites are highly fractionated I-type granites mainly derived from crustal source associated with magma mixing with the lithospheric mantle derived melts. The coeval Tianqiaogou monzodiorites and the Taishanmiao syenogranites support significant curst–mantle interaction in an extensional setting that was related to lithospheric thinning and asthenospheric upwelling in this region. Combined with the widespread granitoids with similar geochemical features of the Taishanmiao syenogranites, large-scale crust–mantle interaction

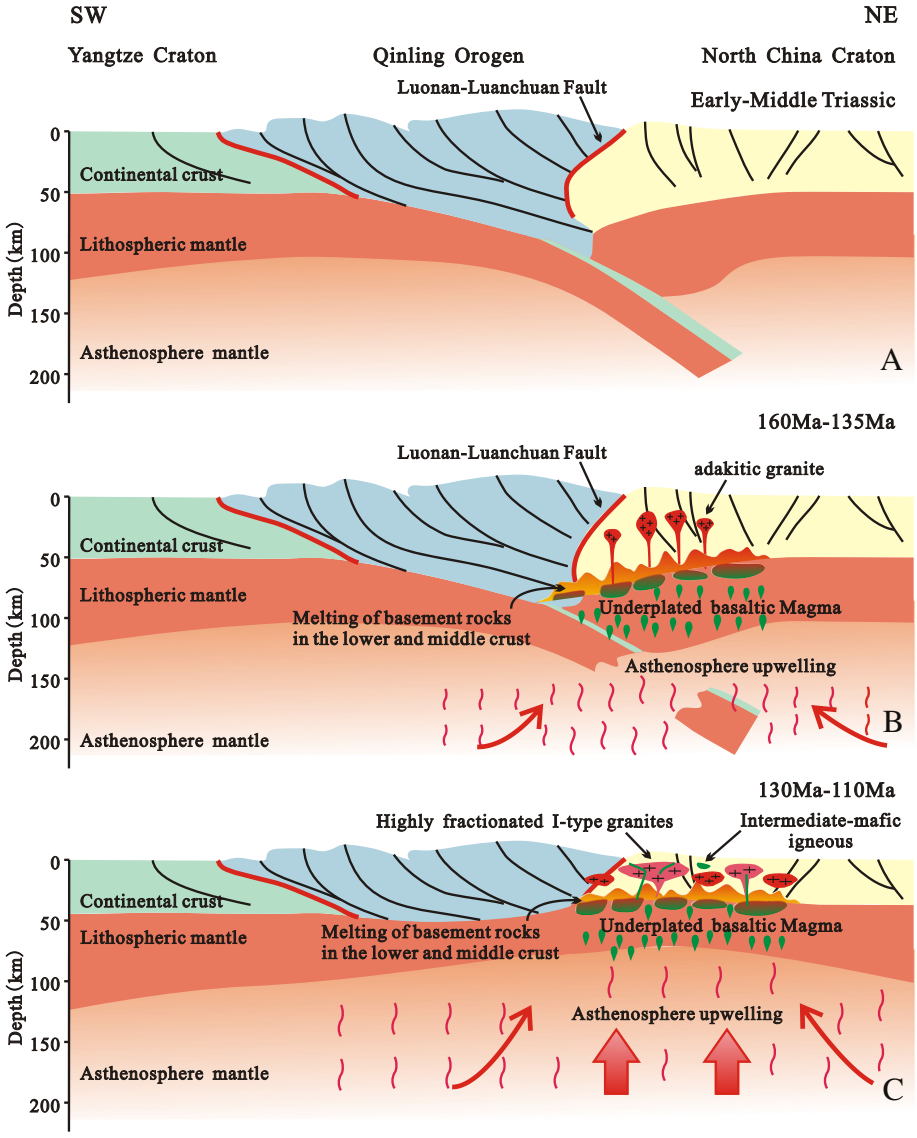

Fig. 12. Tectonic cartoon showing the geodynamic evolution and the formation and development of the magmatic activities in south margin of the NCC. (A) Early–Middle Triassic: Continental collision between the Yangtze and North China Cratons had thickened the lithosphere of the Qinling belt and surrounding areas. (B) 160–135 Ma: The asthenospheric upwelling resulted in inhomogeneous lithospheric thinning with the heat input from underplated mafic magma leading to partial melting of the basement rocks in the overthickened lower crust, producing massive high Ba–Sr granitic intrusions. (C) 130–110 Ma: With progressive melting and thinning, felsic magma chambers were intruded by mantle-derived mafic magmas resulting in varying degrees of magma mixing or mingling. Meantime, the mantle magmas were also emplaced as a dikes or stocks.

and magma underplating are envisaged for the late Mesozoic lithospheric mantle thinning in early Cretaceous in the southern margin of the NCC.

Acknowledgments

This study was funded by the National Natural Science Foundation of China (No. 41373046). We thank Prof. Junhong Zhao and Prof. Cristina Yan Wang for their helpful comments on an early version of the manuscript. We appreciate the assistance of Dr. Jianfeng Gao and Yanyan Zhou for zircon age analyses. We also sincerely thank Dr. Terry Wei Chen and Yonghang Xu for their capable field assistant. We are grateful to two anonymous reviewers and editor in-chief Dr. Andrew Kerr for careful and constructive comments and editorial handling which significantly improved the manuscript. This is contribution No. IS-1935 from GIGCAS.

Appendix A. Supplementary data

Supplementary data to this article can be found online at http://dx.doi.org/10.1016/j.lithos.2014.07.019.

References

Bao, Z.W., Wang, C.Y., Zhao, T.P., Li, C.J., Gao, X.Y., 2014. Petrogenesis of the Mesozoic granites and Mo mineralization of the Luanchuan ore field in the East Qinling Mo mineralization belt, Central China. Ore Geology Reviews 57, 132–153.

Bartolini, A., Larson, R.L., 2001. Pacific microplate and the Pangea supercontinent in the Early to Middle Jurassic. Geology 29, 735–738.

Belousova, E., Griffin, W.L., O'reilly, S.Y., Fisher, N., 2002. Igneous zircon: trace element composition as an indicator of source rock type. Contributions to Mineralogy and Petrology 143, 602–622.

Bergantz, G.W., 1989. Underplating and partial melting: implications for melt generation and extraction. Science 245, 1093–1095.

Cai, Y.C., Fan, H.R., Santosh, M., Liu, X., Hu, F.F., Yang, K.F., Lan, T.G., Yang, Y.H., Liu, Y.S., 2013. Evolution of the lithospheric mantle beneath the southeastern North China Craton: constraints from mafic dikes in the Jiaobei terrain. Gondwana Research 24, 601–621.

Castillo, P.R., Janney, P.E., Solidum, R.U., 1999. Petrology and geochemistry of Camiguin Island, southern Philippines: insights to the source of adakites and other lavas in a complex arc setting. Contributions to Mineralogy and Petrology 134, 33–51.

Chappell, B., 1999. Aluminium saturation in I- and S-type granites and the characterization of fractionated haplogranites. Lithos 46, 535–551.

Chen, Y.J., Guo, G.J., Li, X., 1998. Metallogenic geodynamic background of Mesozoic gold deposits in granite–greenstone terrains of North China Craton. Science in China Series D: Earth Sciences 41, 113–120.

Defant, M.J., Drummond, M.S., 1990. Derivation of some modern arc magmas by melting of young subducted lithosphere. Nature 347, 662–665.
Ding, L.X., Ma, C.Q., Li, J.W., Robinson, P.T., Deng, X.D., Zhang, C., Xu, W.C., 2011. Timing and genesis of the adakitic and shoshonitic intrusions in the Laoniushan complex, southern margin of the North China Craton: implications for post-collisional magmatism associated with the Qinling Orogen. Lithos 126, 212–232.
Diwu, C.R., Sun, Y., Lin, C.L., Li, H.P., Chen, L., Liu, X.M., 2007. Zircon U–Pb ages and Hf isotopes and their geological significance of Yiyang TTG gneisses from Henan Province, China. Acta Petrologica Sinica 23, 253–262 (in Chinese with English abstract).
Diwu, C.R., Sun, Y., Lin, C.L., Wang, H.L., 2010. LA-(MC)-ICPMS U–Pb zircon geochronology and Lu–Hf isotope compositions of the Taihua complex in the southern margin of the North China Craton. Chinese Science Bulletin 55, 2557–2571.
Elburg, M.A., 1996. Evidence of isotopic equilibration between microgranitoid enclaves and host granodiorite, Warburton Granodiorite, Lachlan Fold Belt, Australia. Lithos 38, 1–22.
Falloon, T.J., Green, D.H., Hatton, C.J., Harris, K.L., 1988. Anhydrous partial melting of a fertile and depleted peridotite from 2 to 30 kbar and application to basalt petrogenesis. Journal of Petrology 29, 1257–1282.
Gao, S., Luo, T.C., Zhang, B.R., Zhang, H.F., Han, Y.W., Zhao, Z.D., Hu, Y.K., 1998. Chemical composition of the continental crust as revealed by studies in East China. Geochimica et Cosmochimica Acta 62, 1959–1975.
Gao, S., Rudnick, R.L., Yuan, H.L., Liu, X.M., Liu, Y.S., Xu, W.L., Ling, W.L., Ayers, J., Wang, X.C., Wang, Q.H., 2004. Recycling lower continental crust in the North China craton. Nature 432, 892–897.
Gao, X.Y., Zhao, T.P., Yuan, Z.L., Zhou, Y.Y., Gao, J.F., 2010. Geochemistry and petrogenesis of the Heyu batholith in the southern margin of the North China block. Acta Petrologica Sinica 26, 3485–3506 (in Chinese with English abstract).
Goldfarb, R.J., Santosh, M., 2014. The dilemma of the Jiaodong gold deposits: are they unique? Geoscience Frontiers 5, 139–153.
Griffin, W.L., Wang, X., Jackson, S.E., Pearson, N.J., O'Reilly, S.Y., Xu, X.S., Zhou, X.M., 2002. Zircon chemistry and magma mixing, SE China: in-situ analysis of Hf isotopes, Tonglu and Pingtan igneous complexes. Lithos 61, 237–269.
Guo, P., Santosh, M., Li, S., 2013. Geodynamics of gold metallogeny in the Shandong Province, NE China: an integrated geological, geophysical and geochemical perspective. Gondwana Research 24 (3), 1172–1202.
Hart, S.R., Zindler, A., 1986. In search of a bulk-Earth composition. Chemical Geology 57, 247–267.
He, Y.H., Zhao, G.C., Sun, M., Han, Y.G., 2010. Petrogenesis and tectonic setting of volcanic rocks in the Xiaoshan and Waifangshan areas along the southern margin of the North China Craton: constraints from bulk-rock geochemistry and Sr–Nd isotopic composition. Lithos 114, 186–199.
Hirose, K., Kushiro, I., 1993. Partial melting of dry peridotites at high pressures: determination of compositions using aggregates of diamond. Earth and Planetary Science Letters 114, 477–489.
Huang, X., Wu, L.R., 1990. Nd–Sr isotopes of granitoids from Shanxi Province and their significance for tectonic evolution. Acta Petrologica Sinica 6, 1–11 (in Chinese).
Jahn, B.M., Wu, F., Lo, C.H., Tsai, C.H., 1999. Crust–mantle interaction induced by deep subduction of the continental crust: geochemical and Sr–Nd isotopic evidence from post-collisional mafic–ultramafic intrusions of the northern Dabie complex, central China. Chemical Geology 157 (1), 119–146.
Janoušek, V., Finger, F., Roberts, M., Frýda, J., Pin, C., Dolejš, D., 2004. Deciphering the petrogenesis of deeply buried granites: whole-rock geochemical constraints on the origin of largely undepleted granulites from the Moldanubian Zone of the Bohemian Massif. Transactions of the Royal Society of Edinburgh: Earth Sciences 95, 141–159.
King, P.L., Chappell, B.W., Allen, C.M., White, A.J.R., 2001. Are A-type granites the high-temperature felsic granites? Evidence from fractionated granites of the Wangrah Suite. Australian Journal of Earth Sciences 48 (4), 501–514.
Kröner, A., Compston, W., Zhang, G.W., Guo, A.L., Todt, W., 1988. Age and tectonic setting of Late Archean greenstone–gneiss terrain in Henan Province, China, as revealed by single-grain zircon dating. Geology 16, 211–215.
Le Maitre, R.W., Bateman, P., Dudek, A., Keller, J., Lameyre, J., Le Bas, M.J., Sabine, P.A., Schmid, R., Sorensen, H., 1989. A Classification of Igneous Rocks and Glossary of Terms: Recommendations of the International Union of Geological Sciences Subcommission on the Systematics of Igneous Rocks. Blackwell Scientific Publications, Oxford, pp. 1–193.
Li, Z.X., Li, X.H., 2007. Formation of the 1300 km-wide intracontinental orogen and postorogenic magmatic province in Mesozoic South China: a flat-slab subduction model. Geology 35 (2), 179–182.
Li, S.R., Santosh, M., 2014. Metallogeny and craton destruction: records from the North China Craton. Ore Geology Reviews 56, 376–414.
Li, X.H., Li, W.X., Li, Z.X., 2007. On the genetic classification and tectonic implications of the Early Yanshanian granitoids in the Nanling Range, South China. Chinese Science Bulletin 52, 1873–1885.
Li, J.W., Bi, S.J., Selby, D., Chen, L., Vasconcelos, P., Thiede, D., Zhou, M.F., Zhao, X.F., Li, Z.K., Qiu, H.N., 2012a. Giant Mesozoic gold provinces related to the destruction of the North China craton. Earth and Planetary Science Letters 349, 26–37.
Li, N., Chen, Y.J., Pirajno, F., Gong, H.J., Mao, S.D., Ni, Z.Y., 2012b. LA-ICP-MS zircon U–Pb dating, trace element and Hf isotope geochemistry of the Heyu granite batholith, eastern Qinling, central China: implications for Mesozoic tectono-magmatic evolution. Lithos 142–143, 34–47.
Liu, D.Y., Wilde, S.A., Wan, Y.S., Wang, S.Y., Valley, J.W., Kita, N., Dong, C.Y., Xie, H.Q., Yang, C.X., Zhang, Y.X., Gao, L.Z., 2009. Combined U–Pb, hafnium and oxygen isotope analysis of zircons from meta-igneous rocks in the southern North China Craton reveal multiple events in the Late Mesoarchean–Early Neoarchean. Chemical Geology 261, 140–154.
Ma, L., Jiang, S.Y., Hou, M.L., Dai, B.Z., Jiang, Y.H., Yang, T., Zhao, K.D., Pu, W., Zhu, Z.Y., Xu, B., 2014. Geochemistry of Early Cretaceous calc-alkaline lamprophyres in the Jiaodong Peninsula: implication for lithospheric evolution of the eastern North China Craton. Gondwana Research 25, 859–872.
Mao, J.W., Xie, G.Q., Pirajno, F., Ye, H.S., Wang, Y.B., Li, Y.F., Xiang, J.F., Zhao, H.J., 2010. Late Jurassic–Early Cretaceous granitoid magmatism in Eastern Qinling, central-eastern China: SHRIMP zircon U–Pb ages and tectonic implications. Australian Journal of Earth Sciences 57, 51–78.
Mao, J.W., Pirajno, F., Xiang, J.F., Gao, J.J., Ye, H.S., Li, Y.F., Guo, B.J., 2011. Mesozoic molybdenum deposits in the East Qinling–Dabie Orogenic belt: characteristics and tectonic settings. Ore Geology Reviews 43, 264–293.
Martin, H., 1999. Adakitic magmas: modern analogues of Archaean granitoids. Lithos 46, 411–429.
Ni, Z.Y., Chen, Y.J., Li, N., Zhang, H., 2012. Pb–Sr–Nd isotope constraints on the fluid source of the Dahu Au–Mo deposit in Qinling Orogen, central China, and implication for Triassic tectonic setting. Ore Geology Reviews 46, 60–67.
Patchett, P.J., White, W.M., Feldmann, H., Kielinczuk, S., Hofmann, A.W., 1984. Hafnium/rare earth element fractionation in the sedimentary system and crustal recycling into the Earth's mantle. Earth and Planetary Science Letters 69, 365–378.
Pearce, J.A., Kempton, P.D., Nowell, G.M., Noble, S.R., 1999. Hf-Nd element and isotope perspective on the nature and provenance of mantle and subduction components in Western Pacific arc-basin systems. Journal of Petrology 40 (11), 1579–1611.
Peng, P., Zhai, M.G., Ernst, R.E., Guo, J.H., Liu, F., Hu, B., 2008. A 1.78 Ga large igneous province in the North China craton: the Xiong'er Volcanic Province and the North China dyke swarm. Lithos 101, 260–280.
Rogers, G., Macdonald, R., Fitton, J.G., George, R., Smith, M., Barreiro, B., 2000. Two mantle plumes beneath the East African rift system: Sr, Nd, and Pb isotope evidence from Kenya Rift basalts. Earth and Planetary Science Letters 176, 387–400.
Rudnick, R.L., Fountain, D.M., 1995. Nature and composition of the continental crust: a lower crustal perspective. Reviews of Geophysics 33, 267–309.
Rudnick, R., Gao, S., 2003. Composition of the continental crust. Treatise on Geochemistry 3, 1–64.
Sun, S.S., McDonough, W.F., 1989. Chemical and isotopic systematics of oceanic basalts: implications for mantle composition and processes. Geological Society, London, Special Publications 42, 313–345.
Sun, W.D., Ding, X., Hu, Y.H., Li, X.H., 2007. The golden transformation of the Cretaceous plate subduction in the west Pacific. Earth and Planetary Science Letters 262, 533–542.
Sylvester, P.J., 1998. Post-collisional strongly peraluminous granites. Lithos 45, 29–44.
Tang, Y.J., Zhang, H.F., Santosh, M., Ying, J.F., 2013. Differential destruction of the North China Craton: a tectonic perspective. Journal of Asian Earth Sciences 78, 71–82.
Tian, Y., Zhao, D.P., 2011. Destruction mechanism of the North China Craton: insight from P and S wave mantle tomography. Journal of Asian Earth Sciences 42, 1132–1145.
Vervoort, J.D., Patchett, P.J., Blichert-Toft, J., Albarède, F., 1999. Relationships between Lu–Hf and Sm–Nd isotopic systems in the global sedimentary system. Earth and Planetary Science Letters 168 (1), 79–99.
Wan, Y.S., Wilde, S.A., Liu, D.Y., Yang, C.X., Song, B., Yin, X.Y., 2006. Further evidence for ~1.85 Ga metamorphism in the Central Zone of the North China Craton: SHRIMP U–Pb dating of zircon from metamorphic rocks in the Lushan area, Henan Province. Gondwana Research 9, 189–197.
Wang, T.H., Mao, J.W., Wang, Y.B., 2008. Research on SHRIMP U–Pb chronology in Xiaoqinling–Xionger' shan area: the evidence of delamination of lithosphere in Qinling orogenic belt. Acta Petrologica Sinica 24 (6), 1273–1287 (in Chinese with Engllish abstract).
Wang, X.L., Jiang, S.Y., Dai, B.Z., 2010. Melting of enriched Archean subcontinental lithospheric mantle: evidence from the ca. 1760 Ma volcanic rocks of the Xiong'er Group, southern margin of the North China Craton. Precambrian Research 182, 204–216.
Watson, E.B., Harrison, T.M., 1983. Zircon saturation revisited: temperature and composition effects in a variety of crustal magma types. Earth and Planetary Science Letters 64, 295–304.
Whalen, J.B., Currie, K.L., Chappell, B.W., 1987. A-type granites: geochemical characteristics, discrimination and petrogenesis. Contributions to Mineralogy and Petrology 95, 407–419.
Wolf, M.B., London, D., 1994. Apatite dissolution into peraluminous haplogranitic melts: an experimental study of solubilities and mechanisms. Geochimica et Cosmochimica Acta 58, 4127–4145.
Wu, F.Y., Jahn, B.M., Wilde, S.A., Lo, C.H., Yui, T.F., Lin, Q., Ge, W.C., Sun, D.Y., 2003. Highly fractionated I-type granites in NE China (I): geochronology and petrogenesis. Lithos 66, 241–273.
Wu, F.Y., Lin, J.Q., Wilde, S.A., Zhang, X.O., Yang, J.H., 2005. Nature and significance of the Early Cretaceous giant igneous event in eastern China. Earth and Planetary Science Letters 233, 103–119.
Xiong, X.L., Adam, J., Green, T.H., 2005. Rutile stability and rutile/melt HFSE partitioning during partial melting of hydrous basalt: implications for TTG genesis. Chemical Geology 218, 339–359.
Xu, X.S., Griffin, W.L., Ma, X., O'Reilly, S.Y., He, Z.Y., Zhang, C.L., 2009a. The Taihua group on the southern margin of the North China craton: further insights from U–Pb ages and Hf isotope compositions of zircons. Mineralogy and Petrology 97, 43–59.
Xu, Y.G., Li, H.Y., Pang, C.J., He, B., 2009b. On the timing and duration of the destruction of the North China Craton. Chinese Science Bulletin 54, 3379–3396.
Yang, W., Teng, F.Z., Zhang, H.F., Li, S.G., 2012. Magnesium isotopic systematics of continental basalts from the North China craton: implications for tracing subducted carbonate in the mantle. Chemical Geology 328, 185–194.
Yang, Q.Y., Santosh, M., Shen, J.G., Li, S.R., 2014. Juvenile vs. recycled crust in NE China: zircon U–Pb geochronology, Hf isotope and an integrated model for Mesozoic gold mineralization in the Jiaodong Peninsula. Gondwana Research 25, 1445–1468.

Ye, H.S., Mao, J.W., Xu, L.G., Gao, J.J., Xie, G.Q., Li, X.Q., He, C.F., 2008. SHRIMP zircon U–Pb dating and geochemistry of the Taishanmiao aluminous A-type granite in western Henan Province. Geological Review 54, 699–711.
Zhai, M., Santosh, M., 2013. Metallogeny of the North China Craton: link with secular changes in the evolving Earth. Gondwana Research 24 (1), 275–297.
Zhang, H.F., 2012. Destruction of ancient lower crust through magma underplating beneath Jiaodong Peninsula, North China Craton: U–Pb and Hf isotopic evidence from granulite xenoliths. Gondwana Research 21 (1), 281–292.
Zhang, G.W., Guo, A.L., Liu, F.T., Xiao, Q.H., Meng, Q.R., 1996. Three-dimensional architecture and dynamic analysis of the Qinling orogenic belt. Science in China (Series D) 26, 1–6.
Zhang, H.F., Zhu, R.X., Santosh, M., Ying, J.F., Su, B.X., Hu, Y., 2013. Episodic widespread magma underplating beneath the North China Craton in the Phanerozoic: implications for craton destruction. Gondwana Research 23 (1), 95–107.
Zhao, T.P., Zhai, M.G., Xia, B., Li, H.M., Zhang, Y.X., Wan, Y.S., 2004. Study on the zircon SHRIMP ages of the Xiong'er Group volcanic rocks: constraint on the starting time of covering strata in the North China Craton. Chinese Science Bulletin 9, 2495–2502.
Zhao, D.P., Maruyama, S., Omori, S., 2007. Mantle dynamics of Western Pacific and East Asia: insight from seismic tomography and mineral physics. Gondwana Research 11, 120–131.
Zhao, H.X., Jiang, S.Y., Frimmel, H.E., Dai, B.Z., Ma, L., 2012. Geochemistry, geochronology and Sr–Nd–Hf isotopes of two Mesozoic granitoids in the Xiaoqinling gold district: implication for large-scale lithospheric thinning in the North China Craton. Chemical Geology 294–295, 173–189.
Zhao, J.H., Zhou, M.F., Zheng, J.P., 2013a. Constraints from zircon U–Pb ages, O and Hf isotopic compositions on the origin of Neoproterozoic peraluminous granitoids from the Jiangnan Fold Belt, South China. Contributions to Mineralogy and Petrology 166, 1505–1519.
Zhao, J.H., Zhou, M.F., Zheng, J.P., Griffin, W.L., 2013b. Neoproterozoic tonalite and trondhjemite in the Huangling complex, South China: melting of metasomatised mantle and magma under-plating in a continental arc environment. American Journal of Science 313, 540–583.
Zheng, J.P., Sun, M., Lu, F.X., Pearson, N., 2003. Mesozoic lower crustal xenoliths and their significance in lithospheric evolution beneath the Sino-Korean Craton. Tectonophysics 361, 37–60.
Zheng, J.P., Griffin, W.L., O'Reilly, S.Y., Yu, C.M., Zhang, H.F., Pearson, N., Zhang, M., 2007. Mechanism and timing of lithospheric modification and replacement beneath the eastern North China Craton: peridotitic xenoliths from the 100 Ma Fuxin basalts and a regional synthesis. Geochimica et Cosmochimica Acta 71, 5203–5225.
Zhou, M.F., Chen, W.T., Wang, C.Y., Prevec, S.A., Liu, P.P.P., Howarth, G.H., 2013. Two stages of immiscible liquid separation in the formation of Panzhihua-type Fe–Ti–V oxide deposits, SW China. Geoscience Frontiers 4, 481–502.
Zhu, G., Niu, M.L., Xie, C.L., Wang, Y.S., 2010. Sinistral to normal faulting along the Tan–Lu fault zone: evidence for geodynamic switching of the East China continental margin. The Journal of Geology 118, 277–293.
Zhu, G., Jiang, D.Z., Zhang, B.L., Chen, Y., 2012. Destruction of the eastern North China Craton in a backarc setting: evidence from crustal deformation kinematics. Gondwana Research 22, 86–103.
Zhu, X.Y., Chen, F.K., Liu, B.X., Siebel, W., 2013. Zircon U–Pb and K-feldspar megacryst Rb–Sr isotopic ages and Sr–Hf isotopic composition of the Mesozoic Heyu granite, eastern Qingling orogen, China. Lithos 156–159, 31–40.